INTERNATIONAL JOURNAL FOR NUMERICAL METHODS IN FLUIDS, VOL. 24, 1019–1035 (1997)

# MULTIGRID CONVERGENCE ACCELERATION FOR TURBULENT SUPERSONIC FLOWS

P. GERLINGER[1]* AND D. BRÜGGEMANN[1]

[1]*Institut für Thermodynamik der Luft- und Raumfahrt (ITLR), Universität Stuttgart, Pfaffenwaldring 31, D-70550 Stuttgart, Germany*

## SUMMARY

A multigrid convergence acceleration technique has been developed for solving both the Navier–Stokes and turbulence transport equations. For turbulence closure a low-Reynolds-number $q$–$\omega$ turbulence model is employed. To enable convergence, the stiff non-linear turbulent source terms have to be treated in a special way. Further modifications to standard multigrid methods are necessary for the resolution of shock waves in supersonic flows. An implicit LU algorithm is used for numerical time integration. Several ramped duct test cases are presented to demonstrate the improvements in performance of the numerical scheme. Cases with strong shock waves and separation are included. It is shown to be very effective to treat fluid and turbulence equations with the multigrid method. A comparison with experimental data demonstrates the accuracy of the $q$–$\omega$ turbulence closure for the simulation of supersonic flows. © 1997 by John Wiley & Sons, Ltd. Int. j. numer. methods fluids 24: 1019–1035, 1997.

(No. of Figures: 13. No. of Tables: 0. No. of Refs: 35.)

KEY WORDS: multigrid; supersonic flow; turbulence; $q$–$\omega$ model

## INTRODUCTION

During the last decade, multigrid methods have been widely used for convergence acceleration in a broad range of flow problems.[1–6] They have proved to belong to the most efficient methods to reach a steady state. While first employed for elliptic subsonic flows, this technique may also be applied to supersonic and hypersonic flows.[7–12] However, possible convergence accelerations for high-speed flows seem to be smaller than those achieved for low-speed cases. Using central difference schemes, the kind of artificial viscosity which is responsible for good shock capturing is also a crucial factor for the efficient use of multigrid techniques.[8] While the smoothing of iterative schemes on the finest grid is only efficient within certain ranges of the high-frequency error components, low-frequency errors may be damped on coarser meshes, leading to much better convergence rates. However, high-frequency errors are obtained again by prolongating changes from coarse to fine grids. Therefore the efficiency of multigrid schemes strongly depends on the ability of the driving numerical scheme to rapidly damp out high-frequency errors.[1] In hypersonic flows the efficiency of multigrid is due to the use of larger time steps on coarser grids for damping the long waves while the basic principles of multigrid work on the more dissipation-dominated short waves.[8]

*Correspondence to: P. Gerlinger, Institut für Thermodynamik der Luft- und Raumfahrt (ITLR), Universität Stuttgart, Pfaffenwaldring 31, D-70550 Stuttgart, Germany

Contract grant sponsor: Deutsche Forschungsgemeinschaft (DFG); Contract grant number: SFB 259

CCC 0271–2091/97/101019–17$17.50 *Received May 1996*

Numerical solutions of high-Reynolds-number turbulent flows are often necessary in practical engineering. For turbulence closure, two-equation turbulence models offer a good compromise between accuracy and generality in relation to the necessary computational time and memory. If low-Reynolds-number turbulence models are employed, very fine grids are required for the near-wall regions, making numerical solutions expensive and the use of multigrid techniques attractive. In this case it is advantageous that the necessary number of iterations to reach a steady state be nearly independent of the grid size if multigrid is used for convergence acceleration. However, the turbulence transport equations involve very strongly non-linear source terms, making the use of multigrid methods difficult. In addition, low-Reynolds-number models include exponential functions for the simulation of the near-wall regions. If these terms are treated in the usual way, the solution diverges in most cases. Therefore some authors do not update the turbulence transport equations on coarse grids but only treat the fluid equations with the multigrid scheme.[13,14] Alternatively, a two-level multigrid[15] may be used. Because the solution on the first grid is often very smooth, and the solution on the second grid is driven only by the collected fine grid residuals, a two level multigrid is less critical. However, we found that multilevel multigrid for both the fluid and turbulence transport equations results in the smallest number of necessary multigrid cycles to reach a steady state and in the smallest amount of necessary computer time. This requires a special treatment of the non-linear turbulent source terms.

## FLUID EQUATIONS AND NUMERICAL SCHEME

The investigation of high-speed turbulent flows with massive separation and shock wave–boundary layer interaction requires the solution of the full Navier–Stokes equations which are given in two-dimensional conservation form by

$$\frac{\partial \mathbf{Q}}{\partial t} + \frac{\partial (\mathbf{F} - \mathbf{F}_v)}{\partial x} + \frac{\partial (\mathbf{G} - \mathbf{G}_v)}{\partial y} = 0, \tag{1}$$

where the conservative variable vector is

$$\mathbf{Q} = [\rho, \rho u, \rho v, \rho E, \rho Y_i]^{\mathrm{T}}. \tag{2}$$

$\mathbf{F}$ and $\mathbf{G}$ are the inviscid and $\mathbf{F}_v$ and $\mathbf{G}_v$ the viscous fluxes in the $x$- and $y$-direction respectively. The variables in equation (2) are the density $\rho$, the velocity components $u$ and $v$ in the $x$- and $y$-direction respectively, the total specific energy $E$ and the species mass fractions $Y_i$. Because the code has been developed for the investigation of mixing processes, different species conservation equations are included. The following air calculations require one species conservation equation for oxygen only, while the second mass fraction of nitrogen is the complement to one. Further details may be found in Reference 16.

The unsteady form of the governing equations is integrated in time by using an implicit finite volume LU algorithm[1,17,18]. Jameson and Yoon[19] have demonstrated the property for this driving scheme of rapidly damping out high-frequency modes. This is a basic and necessary feature to be used as a smoother for multigrid methods. Besides the inviscid Jacobians, simplified viscous Jacobians are included in the implicit part of the scheme which are based on the thin layer Navier–Stokes equations. This is done for both fluid and turbulence transport equations. The LU scheme results in block diagonal operators and is fully vectorizable also in the implicit part. The turbulence transport equations are solved in a loosely coupled way with the fluid motion. After linearizing the

 

flux vectors and splitting the inviscid Jacobians to achieve diagonal dominance,[17] the resulting numerical scheme may be symbolically written as

$$(D + L + U)\Delta\mathbf{Q}^{n+1} = -\Delta t\mathbf{R}, \tag{3}$$

where $D$, $L$ and $U$ are a diagonal, a lower triangular and an upper triangular matrix respectively and $\mathbf{R}$ stands for the residual. The implicit operator can be approximately factored as

$$(D + L)D^{-1}(D + U)\Delta\mathbf{Q}^{n+1} = -\Delta t\mathbf{R} \tag{4}$$

and may be solved by the following two steps:[17]

$$\begin{aligned}(D + L)\Delta\bar{\mathbf{Q}} &= -\Delta t\mathbf{R},\\ (D + U)\Delta\mathbf{Q}^{n+1} &= D\Delta\bar{\mathbf{Q}},\\ \mathbf{Q}^{n+1} &= \mathbf{Q}^{n} + \Delta\mathbf{Q}^{n+1}.\end{aligned} \tag{5}$$

Local time stepping is used to enhance convergence to a steady state. The fluid and turbulence transport equations are integrated with the same time step. In many cases the multigrid also allows for larger time steps than the single-grid solution without reaching a stability limit. The following results have been obtained by chosing the same local CFL numbers (between 10 and 20) for all single-grid and multigrid calculations.

As the right-hand side (RHS) is discretized with central differences, second- and fourth-order artificial viscosity is added to reduce oscillations near shock waves and to enable convergence to machine accuracy.[20] This technique is fairly standard; however, a matrix dissipation is employed on the finest grid to reduce the amount of added artificial viscosity.[20,21] While the addition of second-order viscosity is ruled by a pressure-based sensor on the finest grid, only second differences with constant coefficients are added on the coarse grids.[5] With a constant coefficient coarse grid damping, the residuals are kept smooth, limiting high-frequency errors for the prolongation of coarse grid corrections to fine grids. Owing to highly stretched grids in the near-wall region, an anisotropic scaling is necessary for the eigenvalues forming the dissipation matrix.[21] The added artificial viscosity allows one at shock waves to blend over from a second-order central difference scheme to a first-order upwind scheme.[20] In References 7–9 it is shown that the choice of an appropriate shock sensor enables convergence for hypersonic flows without further modifications at shock waves. A similar dissipation is used in the present paper which is described later in more detail.

## THE $q$–$\omega$ TURBULENCE MODEL

In recent years, two-equation turbulence closures have been increasingly employed which use transport equations for a turbulent length and velocity scale. If the turbulence transport equations are integrated directly to the wall, low-Reynolds near-wall corrections are necessary. In contrast with better-behaved wall functions, they are in most cases numerically very stiff. However, low-Reynolds-number models offer a more general application, in particular if flow separation or complex geometries have to be described. If integrated to the wall, the viscous sublayer has to be resolved. Therefore $y^+$-values for the first cells away from the wall should be below unity. Besides a strong increase in the number of necessary grid points, this also leads to highly stretched grids in the near-wall region. For time integration the maximum allowable time step depends on the mesh size of the computational grid. Hence very fine grids in the near-wall regimes require small time steps and increase the number of iterations to reach a steady state. High cell aspect ratios may also lead to a degradation in the damping properties of the driving scheme[22] which can reduce the efficiency of multigrid techniques.

 

If multigrid methods are employed, the strongly non-linear source terms in the boundary layer or within separated regions cause problems which may prevent the solution from converging. Therefore we restricted parts of these terms directly from fine to coarse grids where they were held constant instead of being recalculated.

At described above, most low-Reynolds-number models become numerically extremely stiff in the case of separation or within boundary layers. Therefore we have chosen Coakley's $q$–$\omega$ model[23,24] which behaves much better in such cases and offer high numerical stability.[16,18] Similar properties are observed for the $k$–$\omega$ model[25] developed by Wilcox[26] or the $k$–$\tau$ model of Speziale *et al.*[25] The turbulent transport variables for the $q$–$\omega$ model are $q = \sqrt{k}$ and $\omega = \epsilon/k$, where $k$ is the turbulent kinetic energy and $\epsilon$ is its rate of dissipation. While the asymptotic behaviour for $k$ at solid walls is $\sim y^2$, for $q$ it is $\sim y$. In addition, the use of $q$ instead of $k$ eliminates the need for a low-Reynolds-number dissipation term to balance molecular diffusion.[23] Together with the *ad hoc* boundary condition for $\omega$ at solid walls, $\partial\omega/\partial n = 0$, and the special form of the low-Reynolds-number terms, much of the numerical stiffness associated with low-Reynolds-number turbulence models is eliminated, being a good presumption for the use of multigrid techniques. A further advantage of the $q$–$\omega$ model is the very convenient possibility of flow field initialization with constant freestream values. Even in cases with wall slot injections into supersonic air flows and massive separation in front of and behind the injector, convergence was achieved by this treatment.[16] For the two-dimensional case the field equations for the $q$–$\omega$ model are given by

$$\frac{\partial \mathbf{Q}_{q\omega}}{\partial t} + \frac{\partial(\mathbf{F}_{q\omega} - \mathbf{F}_{q\omega_v})}{\partial x} + \frac{\partial(\mathbf{G}_{q\omega} - \mathbf{G}_{q\omega_v})}{\partial y} = \mathbf{S}_{q\omega}, \tag{6}$$

where

$$\mathbf{Q}_{q\omega} = \begin{bmatrix} \rho q \\ \rho\omega \end{bmatrix}, \qquad \mathbf{F}_{q\omega} = \begin{bmatrix} \rho u q \\ \rho u \omega \end{bmatrix}, \qquad \mathbf{G}_{k\omega} = \begin{bmatrix} \rho v q \\ \rho v \omega \end{bmatrix}, \tag{7}$$

$$\mathbf{F}_{q\omega_v} = \begin{bmatrix} \left(\mu_m + \dfrac{\mu_t}{\sigma_q}\right)\dfrac{\partial q}{\partial x} \\ \left(\mu_m + \dfrac{\mu_t}{\sigma_\omega}\right)\dfrac{\partial \omega}{\partial x} \end{bmatrix}, \qquad \mathbf{G}_{q\omega_v} = \begin{bmatrix} \left(\mu_m + \dfrac{\mu_t}{\sigma_q}\right)\dfrac{\partial q}{\partial y} \\ \left(\mu_m + \dfrac{\mu_t}{\sigma_\omega}\right)\dfrac{\partial \omega}{\partial y} \end{bmatrix}, \tag{8}$$

$$\mathbf{S}_{q\omega} = \begin{bmatrix} C_{q1}\left(C_\mu D_q \dfrac{S}{\omega^2} - \dfrac{2}{3}\dfrac{D}{\omega} - 1\right)\rho\omega q \\ \left[C_{w1}\left(C_\mu \dfrac{S}{\omega^2} - C_{\omega 3}\dfrac{D}{\omega}\right) - C_{\omega 2}\right]\rho\omega^2 \end{bmatrix} \tag{9}$$

and $\mu_m$ and $\mu_t$ are the molecular and the turbulence viscosity respectively. With the strain invariant defined by

$$S = \left[2\frac{\partial u}{\partial x} - \frac{2}{3}\left(\frac{\partial u}{\partial x} + \frac{\partial v}{\partial y}\right)\right]\frac{\partial u}{\partial x} + \left(\frac{\partial u}{\partial y} + \frac{\partial v}{\partial x}\right)^2 + \left[2\frac{\partial v}{\partial y} - \frac{2}{3}\left(\frac{\partial u}{\partial x} + \frac{\partial v}{\partial y}\right)\right]\frac{\partial v}{\partial y} \tag{10}$$

and the divergence of the velocity field defined by

$$D = \frac{\partial u}{\partial x} + \frac{\partial v}{\partial y}, \tag{11}$$

 

the production rate of turbulent kinetic energy is defined by $P_k = \mu_t S - \frac{2}{3}\rho k D$. For modelling the low-Reynolds-number regions, Coakley and Huang[24] introduced the damping functions

$$D_q = 1 - \exp(-0{\cdot}022 R_q) \quad \text{and} \quad C_{\omega 1} = 0{\cdot}5 D_q + 0{\cdot}055 \tag{12}$$

which depend on the turbulent Reynolds number

$$R_q = \rho q l_w / \mu_m. \tag{13}$$

Equation (13) requires the distance $l_w$ from the cell centres to the nearest wall. The basic constants of this model are

$$C_{q1} = 0{\cdot}5, \quad C_{\omega 2} = 0{\cdot}833, \quad C_{\omega 3} = \tfrac{2}{3}, \quad \sigma_q = 0{\cdot}8, \quad \sigma_\omega = 2{\cdot}0, \quad C_\mu = 0{\cdot}09. \tag{14}$$

Finally the eddy viscosity is calculated by

$$\mu_t = C_\mu D_q \rho q^2 / \omega. \tag{15}$$

The boundary conditions at solid walls are $q = 0$ and $\omega_n = 0$, where $n$ is the direction normal to the solid wall. For inflow conditions we used calculated fully developed turbulent inlet profiles for all variables which are held constant. At the exit the primitive variables are extrapolated. Some modifications of this model have been described and investigated in Reference 16. Our main purpose in this paper was the investigation of multigrid in conjunction with a low-Reynolds-number turbulence closure. Therefore the standard $q$–$\omega$ model is employed without investigating the influence of modelling corrections on the numerical accuracy.

## THE MULTIGRID METHOD

For non-linear problems the full approximation storage (FAS) scheme of Brandt[27,28] is the basis for most multigrid methods. In this paper a version for implicit approximately factored schemes is employed which was first presented by Jameson and Yoon.[1] Coarse grids are formed by eliminating every other grid line on the previous finer mesh. In this way a hierarchy of up to four levels $L = h, 2h, 4h, 8h$ of grids is created, where $h$ is the grid size of the finest mesh. A V-cycle with one or two coarse grid iterations is used, starting on the finest grid. In most investigated cases a second coarse grid iteration led only to a small reduction in the number of required multigrid cycles and sometimes even increased the necessary CPU time. Equation (3) may be rewritten in the form

$$F(\mathbf{Q}^k)\Delta\mathbf{Q}^k = \mathbf{R}(\mathbf{Q}^k), \tag{16}$$

where $F$ is the implicit operator, $\mathbf{R}$ is the residual and $k$ indicates the level of the grid. Within one FAS V-cycle the following steps are performed.

*Step 1.* One relaxation sweep is carried out on the finest grid ($k = 1$) according to equation (16) and the solution is updated.

*Step 2.* The solution and the recalculated residuals are transferred from the finest to the next coarse grid by

$$\mathbf{Q}_0^{k+1} = I_k^{k+1}\mathbf{Q}^k, \qquad \mathbf{R}_c^{k+1} = r_k^{k+1}\mathbf{R}(\mathbf{Q}^k), \tag{17}$$

 

where the subscripts '0' and 'c' stand for the initialized coarse grid solution and the collected residuals respectively. $I_k^{k+1}$ and $r_k^{k+1}$ are restriction operators from fine to coarse grids. Now for $k = 1$ a forcing function is defined by[1]

$$\mathbf{P}^{k+1} = \mathbf{R}_c^{k+1} - \mathbf{R}(\mathbf{Q}_0^{k+1}), \tag{18}$$

which is the difference between the transferred residuals from the fine grid and the new calculated coarse grid residuals for which the transferred variables $\mathbf{Q}_0^{k+1}$ are used. The residual for the coarse grid correction is obtained as the sum of the forcing function and the calculated residual,

$$\mathbf{T}^{k+1} = \mathbf{R}(\mathbf{Q}^{k+1}) + \mathbf{P}^{k+1}, \tag{19}$$

and the coarse grid solution is updated using

$$F(\mathbf{Q}^{k+1})\Delta\mathbf{Q}^{k+1} = \mathbf{T}^{k+1}. \tag{20}$$

The first iteration on the second grid is only driven by the collected fine grid residuals. One or more iterations may be performed.

*Step 3.* Again the solution and the recalculated residuals are transferred to the next coarser grid according to equation (17), but the forcing functions for $k > 1$ are now calculated by

$$\mathbf{P}^{k+1} = r_k^{k+1}\mathbf{T}(\mathbf{Q}^k) - \mathbf{R}(\mathbf{Q}_0^{k+1}). \tag{21}$$

Using equation (19), the residual error at the new level $k + 1$ is calculated and the solution updated. Step 3 is repeated successively for every additional level until the coarsest mesh is reached. While the conservative variables are restricted from fine to coarser meshes, the primitive variables, pressure, temperature and gas properties are calculated anew from these transferred values on every coarse grid. The boundary conditions are treated in the same way on all grid levels.

*Step 4.* Finally the obtained coarse grid corrections are prolongated back to the finer grids by

$$\mathbf{Q}_{\text{new}}^k = \mathbf{Q}^k + p_{k+1}^k(\mathbf{Q}_{\text{new}}^{k+1} - \mathbf{Q}_0^{k+1}), \tag{22}$$

where $p_{k+1}^k$ is a prolongation operator from coarse to fine grids. No additional relaxation sweeps are performed on the coarse grids after each prolongation step.

*Restriction and prolongation*

For the cell-centred finite volume scheme used, the restriction operator for the conservative variables is defined according to Reference 1 by

$$I_k^{k+1}\mathbf{Q}^k = \frac{1}{\Omega^{k+1}}\sum_{l=1}^{4} \Omega_l^k\mathbf{Q}_l^k, \tag{23}$$

where $\Omega$ is the corresponding cell area. In this paper, full coarsening is used and always four fine grid volumes are collected to form one coarse grid volume. The residuals $\mathbf{R}$ and $\mathbf{T}$ are restricted by a simple addition of the four fine grid values:

$$r_k^{k+1}\mathbf{R}^k = \sum_{l=1}^{4} \mathbf{R}_l^k, \qquad r_k^{k+1}\mathbf{T}^k = \sum_{l=1}^{4} \mathbf{T}_l^k. \tag{24}$$

Some modifications are necessary if supersonic or hypersonic flows are to be treated. Because central differences are used for space discretization, artificial viscosity is necessary to reduce oscillations near shock waves.[20,21] A pressure-based sensor locates shock waves within the flow field

 

where second differences are added for better shock resolution. Swanson and Turkel[20] proposed a sensor based on the van Leer limiter which is first-order upwind near shocks and has total-diminishing (TVD) properties. In the following calculations we use an arithmetic blend ($\chi = 0{\cdot}5$) between the original[29] non-TVD ($\chi = 1$) and the TVD ($\chi = 0$) sensor

$$v^{\xi}_{i,j} = \frac{|p_{i+1,j} - 2p_{i,j} + p_{i-1,j}|}{(1-\chi)(|p_{i+1,j} - p_{i,j}| + |p_{i,j} - p_{i-1,j}|) + \chi(p_{i+1,j} + 2p_{i,j} + p_{i-1,j})}, \tag{25}$$

which is given here for the $\xi$-direction. Similar sensors are used by other authors for multigrid calculations in hypersonic flows.[8–10] In addition, fourth-order viscosity is added in the smooth flow regions to prevent odd–even oscillations and to allow convergence to machine accuracy. The fourth-order dissipation is switched off near shock waves.

Because this kind of dissipation and a central restriction operator still allow for upwind propagation of disturbances, the residuals transferred from fine to coarse grids are damped in the vicinity of shock waves.[10] A different but more complicated possibility would be a characteristic restriction operator as proposed by Leclercq and Stoufflet[30] which requires computationally expensive matrix–vector multiplications. To locate regions where the transferred residuals should be reduced, shock sensors in the $\xi$- and $\eta$-directions are used,[10]

$$\kappa^{k}_{i,j} = C^{k} \max(v^{\xi}_{i,j}, v^{\xi}_{i-1,j}, v^{\xi}_{i+1,j}, v^{\eta}_{i,j}, v^{\eta}_{i,j-1}, v^{\eta}_{i,j+1}), \tag{26}$$

and equation (24) is replaced by

$$r^{k+1}_{k}\mathbf{R}^{k} = \sum_{l=1}^{4} \mathbf{R}^{k}_{l} \max(0, 1 - \kappa^{k}_{l}), \qquad r^{k+1}_{k}\mathbf{T}^{k} = \sum_{l=1}^{4} \mathbf{T}^{k}_{l} \max(0, 1 - \kappa^{k}_{l}). \tag{27}$$

On the finest grid the pressure distribution is normally smooth and even at shock waves the values of $\kappa_{i,j}$ are relatively small if the grid is fine enough and the shock wave is not too strong. This behaviour changes on coarse grids where stronger pressure gradients occur, leading to higher values of $\kappa_{i,j}$. Therefore it may be advantageous to take different values of $C^{k}$ for the different grid levels $k$. For coarser grids, smaller values allow more information to pass and allow better convergence rates. In addition, it is important to notice that the transferred residuals are multiplied by the damping factor at every grid transfer, leaving less information on successively coarser grids.

With an implicit scheme, information is propagated through the shock wave even if $\mathbf{R}^{k}$ becomes zero directly at the shock. However, corrections obtained near shock waves and prolongated to finer grids may be too large in some phases of the iteration process and may lead to divergence of the calculation. This effect was described in Reference 10 and is also observed in our calculations. Therefore, in addition to the above-described reduction of the restricted residuals, the local time steps for the coarse grid calculations are reduced at shock waves in dependence on the value of $\kappa_{i,j}$.

For the prolongation of corrections from coarse to fine grids, bilinear interpolation is used. Similar to the restriction process, such a central prolongation operator may allow for unphysical upwind propagation of disturbances in supersonic flows. In our first test case this was less critical because a very fine grid was used. Machine accuracy could be achieved with a central prolongation operator. However, for calculations with coarser grids we required an upwind prolongation which was used only in supersonic flow regions. The contravariant velocity between two coarse grid cell centres is used as a sensor to switch between upwind and central prolongation if supersonic or subsonic flow exists between those two points. Again Leclercq and Stoufflet[30] describe a more accurate characteristic prolongation. However, the computational effort is much larger for such a treatment and good results have been obtained with the described simple switching.

 

*The turbulent source terms*

If the turbulent source vector described in equation (9) is recalculated with restricted coarse grid variables, the strong non-linear character of some included terms may lead to divergence of the calculation. This is especially the case for massively separated flows which are associated with strong gradients in the flow and turbulence variables. To preserve the accuracy of the source term, it is possible to directly pass down these values from fine to coarse grids without a new calculation. Such a method conserves the turbulent variables. If an implicit numerical scheme is used, it is necessary to form a source Jacobian on every grid according to the source vector. Especially for the low-Reynolds-number terms it may be difficult to find a formulation which enables rapid convergence if the whole source terms is passed down. Therefore another possibility is chosen which requires no modification for the calculation of the turbulent source Jacobian on coarse grids. The strongest non-linear terms of the source vector given in equation (9) are the production rate $P_k$ which is formed by $S$ and $D$ and the exponential function $D_q$. If these terms are recalculated on the coarse grids, their non-linear behaviour may destroy convergence. Therefore they are restricted in the way as the conservative variables from fine to coarser grids, i.e.

$$S^{k+1} = I_k^{k+1} S^k, \qquad D^{k+1} = I_k^{k+1} D^k, \qquad D_q^{k+1} = I_k^{k+1} D_q^k, \tag{28}$$

and are held constant for every coarse grid iteration. The turbulent source Jacobians are calculated with the frozen restricted values of $S, D$ and $D_q$. It is advantageous that all terms which are held constant on the coarse grids be independent of $q$ and $\omega$. The turbulence variables change during the multigrid cycle on the coarse grids, while approximations are used for the strong non-linear parts of the source vector which are determined from exact fine grid values. While is important to treat $S$ and $D_q$ in the above-described way, $D$ is less critical and may also be recalculated on the coarse grids. However, for simplicity we used constant values for all three terms and achieved good convergence rates even for complicated flow fields. The source Jacobian for the $q$–$\omega$ model may be found in Reference 18.

## RESULTS AND DISCUSSION

Several test cases have been achieved to investigate the convergence acceleration of the described multigrid scheme and to demonstrate the accuracy of the low-Reynolds-number $q$–$\omega$ model for the simulation of attached and separated supersonic flows. In all cases, significant grid clustering is necessary to resolve the viscous sublayers near solid walls, leading to highly stretched grids with cell aspect ratios up to 500. While the first test case is only used to investigate the convergence properties of the numerical scheme, a comparison with experimental data has been made for a series of ramp flows, from which the most complicated one is presented.

*Ramped duct without separation*

A simple ramped duct test case serves to investigate the convergence properties of the above-described multigrid method. Figure 1 shows the geometry and inflow conditions, which are the same as those used for the investigation of supersonic combustion problems.[31] A small fully developed turbulent boundary layer with a boundary layer thickness $\delta = 0{\cdot}3$ mm is used at the inlet. This assures that no separation is induced by the shock wave at the ramp. Because the computational grid with $120 \times 80$ volumes is very fine for the small geometry, owing to its good resolution, this test case is less critical than the following ones. A constant value of $C^k = 1$ is used (see equation (26)) for all grids, leading at stationary conditions to maximum values for $\kappa_{i,j}$ of 0·0583, 0·1121 and 0·1771 for

 

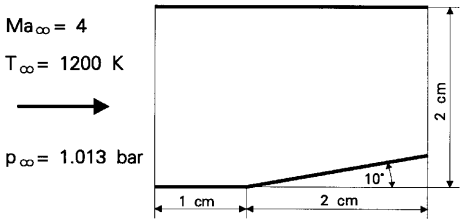


Figure 1. Geometry and inflow conditions for ramped duct

the first, second and third grids respectively. For this case it was not necessary to reduce the coarse grid time steps at the shock or to use the upwind prolongation. The computational grid is refined near the lower and upper walls and all $y^+$-values for the first cell centres away from the wall are below unity. All converged single-grid and multigrid solutions are identical.

The calculations presented in this paper have been performed on a Cray C90 computer with a fully vectorized code. Because of the short vector lengths on coarse grids, the necessary computer time increases more strongly than the theoretically achievable value if the multigrid method is employed. The implicit part of the LU scheme which is vectorized along the diagonals of the computational domain is at a special disadvantage, because the maximum vector length is given by the smallest number of cells in both co-ordinate directions. For three-dimensional calculation the vectorization may be performed in planes, which offers much longer vector lengths and improves the performance rate.[5] In addition, the vector length increases quadratically instead of linearly starting from one corner of the computational domain until the maximal vector length is reached. Therefore still better accelerations may be expected for three-dimensional calculations or if a scalar computer is used.

Figures 2 and 3 show the convergence histories for various calculations. The absolute, averaged, normalized residual errors of the continuity equation are given for four different calculations as a function of the number of multigrid cycles or work units respectively. One work unit represents the computational effort for one fine grid iteration. The necessary number of iterations as well as the number of work units is strongly reduced by the four-level V-cycle multigrid method. In order to demonstrate the advantage of treating the turbulence equations with the multigrid method, two

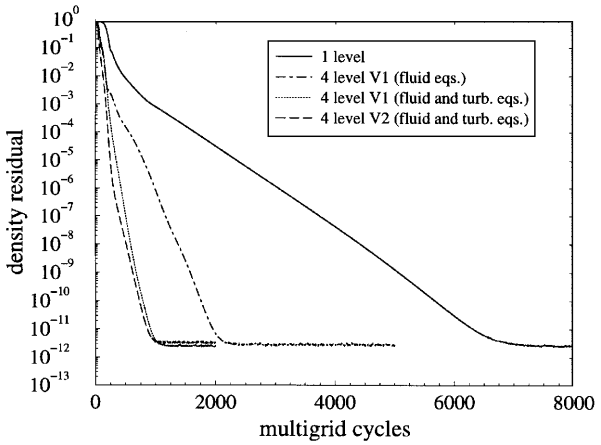


Figure 2. Convergence history (multigrid cycles) for density residual

 

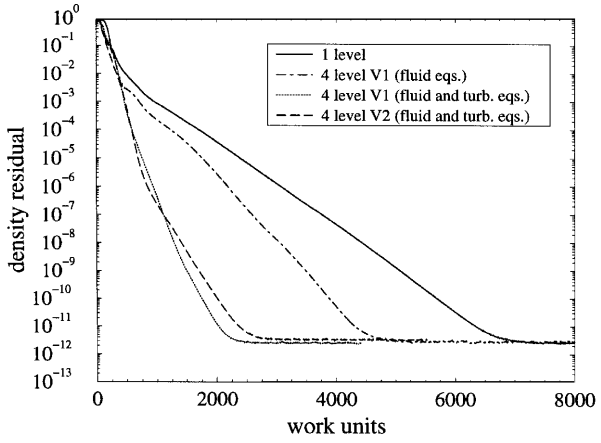


Figure 3. Convergence history (work units) for density residual

different calculations are performed with four levels and one coarse grid iteration. While in the first simulation the multigrid method is used only for the fluid equations in the second, it serves for both the fluid and turbulence transport equations. From these results (see Figures 2 and 3) it is obvious that further improvements are achieved if all equations are treated with the multigrid technique. If may also be seen from these figures that in this case a second coarse grid iteration only achieves a very small reduction in the number of multigrid cycles, while the number of work units is even increased.

Figures 4 and 5 show the convergence histories of the absolute, averaged, normalized residual errors of the $q$-equation. The advantage of treating the turbulence transport equations with the multigrid method becomes still clearer from these figures. While machine accuracy is reached at the same number of work units (2750) for the $\rho$- and the $q$-residual if all equations are treated with the multigrid, the convergence of $q$ is lagged if only the fluid equations are treated. In this case the density residual reaches machine accuracy after 4750 work units, while 5700 are necessary for the $q$-residual. At the beginning of the iteration the number of work units is even increased by the multigrid technique in comparison with the single-grid solution if only the fluid equations are treated.

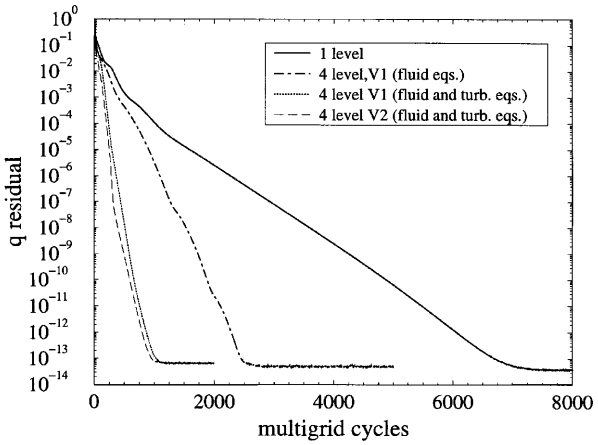


Figure 4. Convergence history (multigrid cycles) for $q$-residual

 

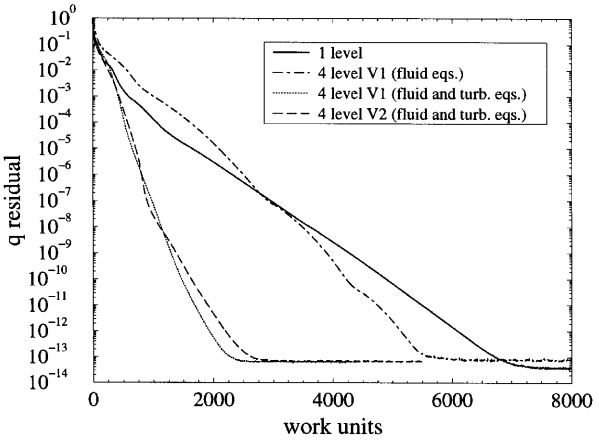


Figure 5. Convergence history (work units) for $q$-residual

A convergence acceleration with a factor of about 3·5 concerning the number of necessary work units is achieved when the four-level V-cycle multigrid is used for the fluid and turbulence transport equations. It will be shown in the next subsection that still stronger accelerations are possible in the case of massive separation, where the single-grid solutions slow down.

*24° ramp with separation*

The following test case was performed experimentally by Settles and co-workers[32–34] and is often used for the investigation of turbulence models because of its good documentation. This case is more challenging to the multigrid scheme as well as to the turbulence closure than the previous one because of the strong shock wave–boundary layer interactions and the associated flow field separation. The geometry and computational grid for the flow over a planar 24° compression corner as well as the freestream inflow conditions given in Figure 6. The inflow boundary conditions have been calculated by the same Navier–Stokes code to match the experimentally measured[32] boundary layer thickness $\delta = 2{\cdot}1$ cm, displacement thickness $\delta^* = 0{\cdot}602$ cm and momentum thickness $\theta = 0{\cdot}114$ cm as were as possible. These profiles also serve as initial conditions throughout the computational domain. Four different compression corners have been investigated experimentally (8°, 16°, 20° and 24°). While calculations have been performed for all four ramp angles, results will be presented only for the 24° ramp where the largest separation zone occurs. However, even though not shown in this paper, the convergence rates as well as the overall agreement with the experimental data are also very good for the other ramp flows. Adiabatic wall boundary conditions are assumed for all calculations. The computational grid (152 × 80 volumes) shown in refined near the corner and at the solid wall and the distance from the first cell centre to the wall is $0{\cdot}5 \times 10^{-6}$ m, leading to $y^+$-values below 0·6 for all near-wall cell centres. In the mean the flow was found in experiment to separate at $x = -34$ mm and to reattach at $x = 11$ mm.[35]

Figures 7 and 8 show the performance parameters for this calculation. It may be seen that the fluid and turbulence transport equations converge at nearly the same rate. Again a strong reduction in the necessary number of multigrid cycles or work units is demonstrated. Fewer than 5000 multigrid cycles are required to achieve machine accuracy in the case of the multigrid V-cycle with two coarse grid iterations. For the 8°, 16° and 20° ramps the convergence rates are a little bit better still. The necessary CPU time on a single processor of the Cray C90 is about 16 $\mu$s per grid point per iteration. For this pure air calculation a multicomponent algorithm is disadvantageous as it requires

 

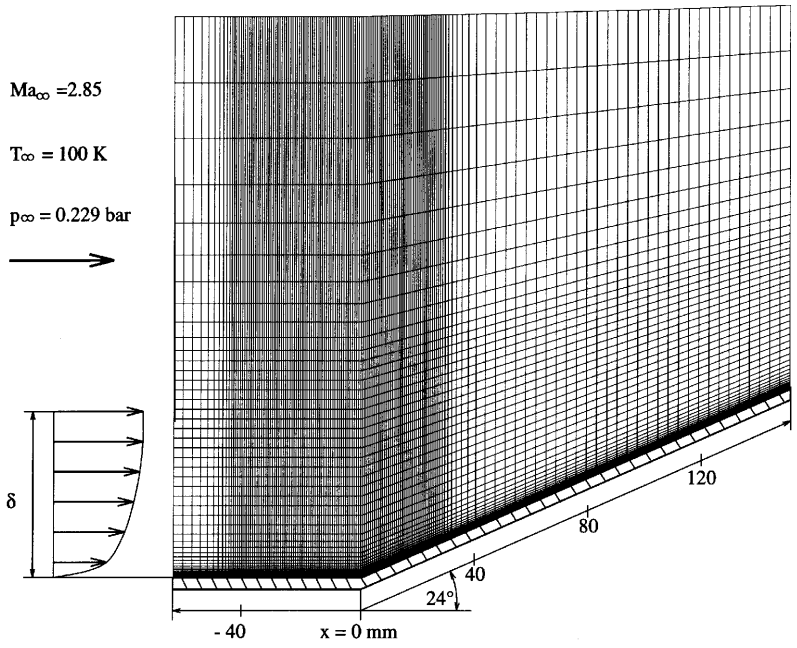


Figure 6. Geometry, inflow conditions and computational grid (152 × 80)

complicated gas property calculations. In comparison with the first test case, now a second coarse grid iteration achieves a clearly visible improvement in the convergence rates. Again a constant value of $C^k = 1$ is used for all grids, leading at stationary conditions to maximum values for $\kappa_{i,j}$ of 0·103, 0·252 and 0·346 for the first, second and third grids respectively. In addition, the CFL number is also reduced in regions with strong pressure gradients, leading to minimum multiplicators of 0·924, 0·784 and 0·699 for the time step size on the second, third and fourth grids respectively. It is also possible to achieve convergence without reducing the time step size but by increasing $C^k$. The convergence rates

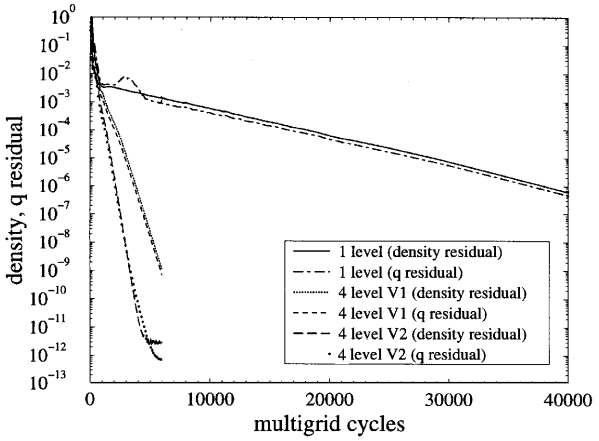


Figure 7. Convergence history (multigrid cycles) for density residual and *q*-residual

 

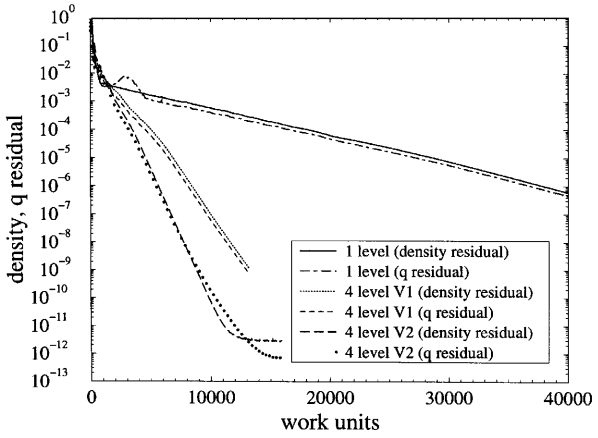


Figure 8. Convergence history (work units) for density residual and $q$-residual

differ only slightly. Both methods are stable and simple to use. There is no influence on the stationary solution if $C^k$ is chosen too large, but the convergence slows down.

Figure 9 shows a comparison between the experimental (two sets of measurements)[24,31] and computed wall static pressures. The overall agreement between experimental and computation is quite good. The computational rise in pressure due to the separation shock is somewhat steeper than in the experiment. The computed and experimentally determined skin friction coefficients are plotted in Figure 10. While the computed point of separation agrees very well with the measured value, the point of reattachment is further downstream for the calculation. Additionally, the calculated rise in skin friction at the beginning of and after reattachment is steeper than in the experiment. The wrongly predicted point of reattachment may also be seen in the velocity profiles which are given in Figure 11 for eight different $x$-locations. The profiles are always plotted vertical to the ramp surface. Substantial difference occur especially within the separated region. Finally, Figures 12 and 13 show the pressure distribution and $q$-distribution within the computational domain respectively. There is a strong production of turbulent kinetic energy near the ramp and within the separated region. The maximum

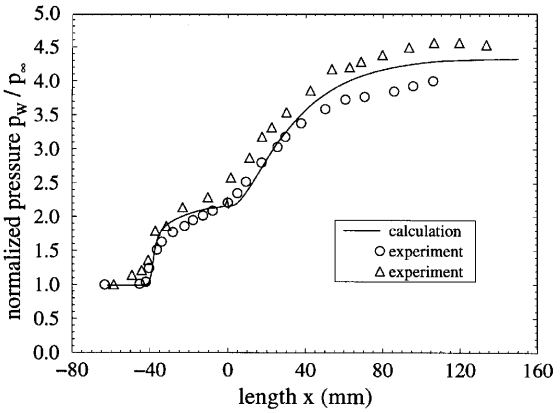


Figure 9. Experimental and computed surface static pressure distribution

 

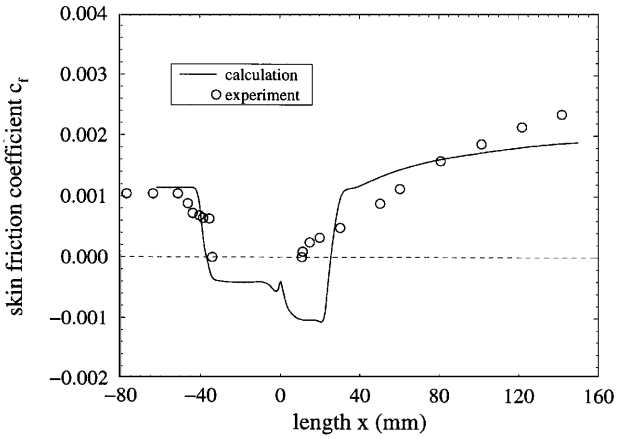


Figure 10. Experimental and computed surface skin friction distribution $c_f = 2\tau_W/\rho_\infty u_\infty^2$

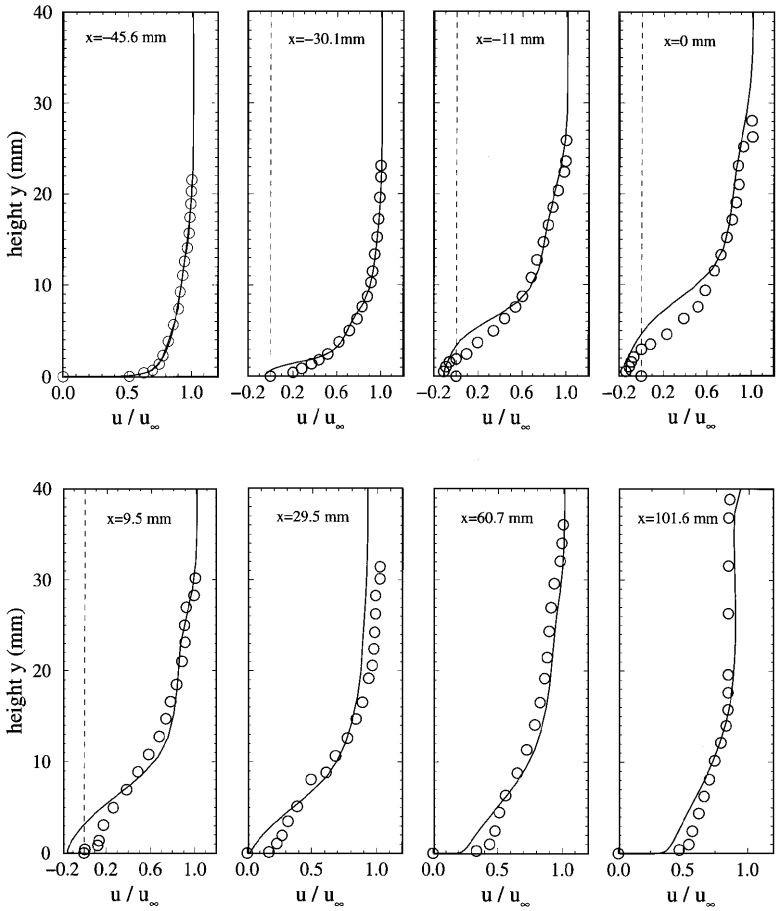


Figure 11. Experimental and computed velocity profiles at various $x$-locations

 

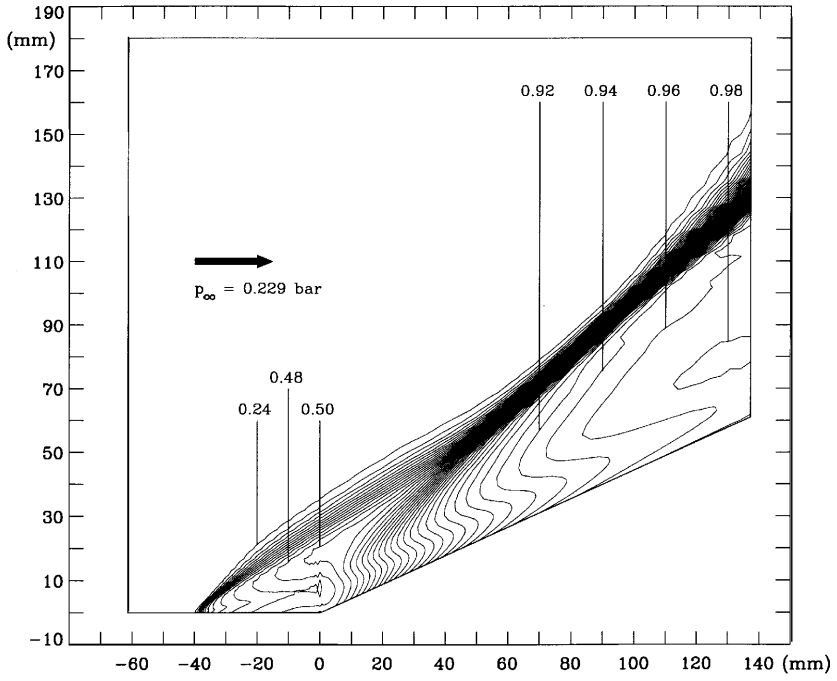


Figure 12. Pressure contours (bar) for computational domain ($\Delta = 0{\cdot}02$ bar)

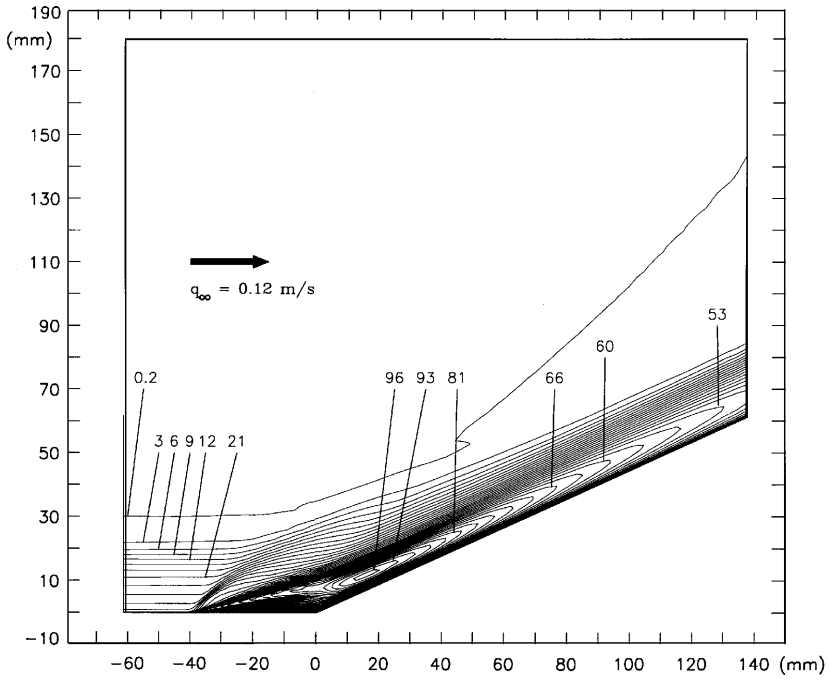


Figure 13. Contours of $q$ (m s$^{-1}$) for computational domain ($\Delta = 3$ m s$^{-1}$)

 

values are obtained at about $x = 20$ mm, decreasing again further downstream towards a fully turbulent boundary layer profile.

Despite the described differences between experiment and calculation, the overall agreement is still satisfactory for a two-equation turbulence closure, as may also be seen from comparison with the results of other authors.[24,26]

## CONCLUSIONS

The multigrid technique was successfully introduced to accelerate convergence for supersonic flows using a $q$–$\omega$ low-Reynolds-number turbulence model. It has been shown that it is advantageous to use the multigrid technique for both the fluid and turbulence transport equations. A method for treating the non-linear turbulent source terms is presented which leads to a simple coarse grid source Jacobian approximation necessary for implicit schemes. In addition, restriction and prolongation between the different grid levels requires a special treatment near shock waves to enable convergence. The $q$–$\omega$ model has proven to be numerically very stable in conjunction with the multigrid technique and a comparison with experimental results has shown good overall agreement.

### ACKNOWLEDGEMENT

We would like to thank the Deutsche Forschungsgemeinschaft (DFG) for financial support of this work within the special research programme SFB 259 at the University of Stuttgart.

### REFERENCES

1. A. Jameson and S. Yoon, 'Lower–upper implicit schemes with multiple grids for the Euler equations', *AIAA J.*, **25**, 929–935 (1987).
2. L. Martinelli, A. Jameson and F. Grasso, 'A multigrid method for the Navier–Stokes equations', *AIAA Paper 86-0208*, 1986.
3. G. A. Gerolymos, 'Implicit multiple-grid solution of the compressible Navier–Stokes equations using $k$–$\epsilon$ turbulence closure', *AIAA J.*, **28**, 1707–1717 (1990).
4. W. A. Mulder, 'A high-resolution Euler solver based on multigrid, semi-coarsening and defect correction', *J. Comput. Phys.*, **100**, 91–104 (1992).
5. S. Yoon and D. Kwak, 'Multigrid convergence of an implicit symmetric relaxation scheme', *AIAA J.*, **32**, 950–955 (1994).
6. P. W. Hemker and B. Koren, 'Defect correction and nonlinear multigrid for the Euler equations', *Lecture Series 1988-05*, von Karman Institute for Fluid Dynamics, 1988.
7. R. C. Swanson, E. Turkel and J. A. White, 'An effective multigrid method for high-speed flows', *NASA ICASE Rep. 91-56*, 1991.
8. E. Turkel, R. C. Swanson, V. N. Vatsa and J. A. White, 'Multigrid for hypersonic viscous two- and three-dimensional flow', *NASA ICASE Rep. 91–57*, 1991.
9. V. N. Vatsa, E. Turkel and J. S. Abolhassani, 'Extension of multigrid methodology to supersonic/hypersonic 3-D viscous flows', *Int. j. numer. methods fluids*, **17**, 825–837 (1993).
10. R. Radespiel and R. C. Swanson, 'Progress with multigrid schemes for hypersonic flow problems', *J. Comput. Phys.*, **116**, 103–122 (1995).
11. J. R. Edwards, 'Development of an upwind relaxation multigrid method for computing three-dimensional, viscous internal flows', *AIAA Paper 95-0208*, 1995.
12. J. R. Edwards, 'An implicit multigrid algorithm for computing hypersonic, chemically reacting viscous flows', *J. Comput. Phys.*, **123**, 84–95 (1996).
13. J. W. Yokota, 'A diagonally inverted LU implicit multigrid scheme for the 3-dimensional Navier–Stokes equations and a two equation model of turbulence', *NASA CR 182209*, 1988.
14. E. Dick, P. Herbosch, J. Steelant and C. Lacor, 'Comparison of multigrid solutions of the compressible Navier–Stokes equations coupled to the $k$–$\epsilon$ turbulence equations for upwind and central difference schemes', *Proc. ECOMAS 2nd Eur. Computational Fluid Dynamics Conf.*, Vol. 1, 1994, pp. 356–362.
15. A. A. Ameri and A. Arnone, 'Navier–Stokes turbine heat transfer predictions using two-equations turbulence closures', *AIAA Paper 92-3067*, 1992.

 

16. P. Gerlinger, J. Algermissen and D. Brüggemann, 'Numerical simulation of mixing for turbulent slot injection', *AIAA J.*, **34**, 73–78 (1996).
17. J. S. Shuen, 'Upwind differencing and LU factorization for chemical non-equilibrium Navier–Stokes equations', *J. Comput. Phys.*, **99**, 233–250 (1992).
18. P. Gerlinger and J. Algermissen, 'Numerical simulation of supersonic combustion problems using an implicit LU-SGS scheme and $k$–$\epsilon/q$–$\omega$ turbulence closure', *AIAA Paper 93-5021*, 1993.
19. A. Jameson and S. Yoon, 'Multigrid solution of the Euler equations using implicit schemes', *AIAA J.*, **24**, 1737–1743 (1986).
20. R. C. Swanson and E. Turkel, 'On central difference and upwind schemes', *J. Comput. Phys.*, **101**, 292–306 (1992).
21. P. Gerlinger, J. Algermissen and D. Brüggemann, 'Matrix dissipation for central difference schemes with combustion', *AIAA J.*, **33**, 1865–1870 (1995).
22. J. R. Edwards, 'Upwind relaxation multigrid method for computing three-dimensional, viscous internal flows', *J. Prop. Power*, **12**, 146–154 (1996).
23. T. J. Coakley, 'Turbulence modeling methods for the compressible Navier–Stokes equations', *AIAA Paper 83-1693*, 1983.
24. T. J. Coakley and P. G. Huang, 'Turbulence modeling for high speed flows', *AIAA Paper 92-0436*, 1992.
25. C. G. Speziale, R. Abid and E. C. Anderson, 'Critical evaluation of two-equation models for near-wall turbulence', *AIAA J.*, **30**, 324–331 (1992).
26. D. C. Wilcox, 'Reassessment of the scale-determining equation for advanced turbulence models', *AIAA J.*, **26**, 1299–1310 (1988).
27. A. Brandt, 'Multi-level adaptive solutions to boundary-value problems', *Math. Comput.*, **31**, 333–390 (1977).
28. A. Brandt, 'Multi-level adaptive solutions in fluid dynamics', *INKA-Conf.-79, 351–010, 79–1455*, 1979.
29. A. Jameson, W. Schmidt and E. Turkel, 'Numerical solution of the Euler equations by finite volume methods using Runge–Kutta time stepping schemes', *AIAA Paper 81-1259*, 1981.
30. M. P. Leclerq and B. Stoufflet, 'Characteristic multigrid method application to solve the Euler equations with unstructured and unnested grids', *J. Comput. Phys.*, **104**, 329–346 (1993).
31. J. S. Shuen and S. Yoon, 'Numerical study of chemically reacting flows using an lower–upper successive overrelaxation scheme', *AIAA J.*, **27**, 1752–1760 (1989).
32. G. S. Settles, I. E. Vas and S. Bogdonoff, 'Details of a shock-separated turbulent boundary layer at a compression corner', *AIAA J.*, **14**, 1709–1715 (1976).
33. G. S. Settles, T. J. Fitzpatrick and S. Bogdonoff, 'Detailed study of attached and separated compression corner flowfields in high Reynolds number supersonic flow', *AIAA J.*, **17**, 579–585 (1979).
34. E. Reshotko (ed.), 'A survey of measurements and measuring techniques in rapidly distorted compressible turbulent boundary layers', *AGARD-AG-315*, 1989, pp. 12A-1–12A-16.
35. M. S. Selig, J. Andreopoulos, K. C. Muck, J. P. Dussauge and A. J. Smits, 'Turbulence structure in a shock wave/turbulent boundary-layer interaction', *AIAA J.*, **27**, 862–869 (1989).

 